minerals

MDPI

Review

Structural Principles of Ion-Conducting Mineral-like Crystals with Tetrahedral, Octahedral, and Mixed Frameworks

Dmitry Pushcharovsky [1,*] and Alexey Ivanov-Schitz [2]

[1] Geological Faculty, Lomonosov Moscow State University, Leninskie Gory 1, Moscow 119991, Russia
[2] Kurchatov Complex of Crystallography and Photonics (KCCF), National Research Center "Kurchatov Institute", Leninsky Pr. 59, Moscow 117333, Russia; alexey.k.ivanov@gmail.com
* Correspondence: dmitp@geol.msu.ru

Abstract: Materials with high ion mobility are widely used in many fields of modern science and technology. Over the last 40 years, they have thoroughly changed our world. The paper characterizes the structural features of minerals and their synthetic analogs possessing this property. Special attention is paid to the ionic conductors with tetrahedral (zincite- and wurtzite-like), octahedral (ilmenite-like), and mixed (NASICON-like) frameworks. It is emphasized that the main conditions for fast ionic transport are related to the size and positions occupied by a mobile ion, their activation energy, the presence and diameter of conduction channels running inside the structure, isomorphic impurities, and other structural peculiarities. The results of the studies of solid electrolytes are dispersed in different editions, and the overview of new ideas related to their crystal structures was the focus of this paper.

Keywords: ionic conductivity; structural types of superionic crystals; heterovalent isomorphism in ionic conductors; ionic conductors among minerals and their synthetic analogs

check for updates

Citation: Pushcharovsky, D.; Ivanov-Schitz, A. Structural Principles of Ion-Conducting Mineral-like Crystals with Tetrahedral, Octahedral, and Mixed Frameworks. *Minerals* **2024**, *14*, 770. https://doi.org/10.3390/min14080770

Academic Editor: Bojan A. Marinković

Received: 28 June 2024
Revised: 23 July 2024
Accepted: 24 July 2024
Published: 29 July 2024

Copyright: © 2024 by the authors. Licensee MDPI, Basel, Switzerland. This article is an open access article distributed under the terms and conditions of the Creative Commons Attribution (CC BY) license (https://creativecommons.org/licenses/by/4.0/).

1. Introduction

The first references to the high conductivity of ionic crystals date back to the early 19th century [1]. In 1833, M. Faraday noted [2] the anomalously high electrical conductivity of PbF_2 and Ag_2S, comparable to metals. Both compounds are characterized by existence of polymorphic modifications. Fluorocronite, PbF_2, is a cubic fluorite-type natural analog of β-PbF_2, which is stable at environmental conditions and shows a conductivity 2.4 S·cm^{-1} at 1000 K. Orthorhombic α-PbF_2 with cotunnite ($PbCl_2$) structure is more stable at higher pressures. Ag_2S has three polymorphs: low-temperature monoclinic (space group $P2_1/c$) α-Ag_2S (natural analog acanthite) exists at temperatures below 450 K, body-centered cubic (space group *Im*-3*m*) superionic β-Ag_2S (argentite) exists in the temperature range of 452–860 K, and the high-temperature face-centered cubic (space group *Fm*3*m*) γ-Ag_2S phase is stable at T > 860 K [3]. The conductivity of β-Ag_2S at room temperature is (1.3–1.6) × 103 S·cm^{-1}, and at elevated temperature range it exceeds 5 S·cm^{-1} [4,5]. A similar effect in oxide materials was discovered by W. Nernst in 1897, who used ceramics based on zirconium oxide ZrO_2 doped with yttrium (Y_2O_3) as a material for incandescent lamps [6].

In the early 20th century, scientists proved that the high conductivity of such substances was due to the movement of different ions rather than electrons, as observed in liquid electrolytes. Under normal conditions, the ion transport in ordinary solids—both crystalline and amorphous—is not very significant, and at room temperature, the specific conductivity does not exceed 10^{-10}–10^{-12} S·cm^{-1} (the siemens (symbol: S) is the unit of electric conductance in the International System of Units (SI); one siemens is equal to the reciprocal of one ohm (Ω^{-1})). There exist many solids with high ionic conductivity > 10^{-4} S·cm^{-1} [7]. There are two main groups of crystals that exhibit this physical property. The first group includes superionic conductors, also called fast ion conductors or solid electrolytes, whose

conductivity is several orders higher and lies in the range of 10^{-3} S·cm^{-1} to 10 S·cm^{-1}. These values are very high for crystalline ionic solids but are still lower than those of many electronic conductors, such as metals, which have typical values ranging from 10 to 10^5 S·cm^{-1} [8].

Superionic conductors have high ionic conductivity because of strong disorder in the sublattice of conducting ions. There are crystals with so-called impurity-induced structure disorder. In these solids, the conductivity is due to a high concentration of impurity ions, which promote the disordering of the structure.

The main general requirements for the practical use of solid electrolytes are as follows: (1) High ionic conductivity; (2) Negligible electronic conductivity; (3) Stability with respect to adjacent phases and thermal and electrochemical decomposition [9].

High ionic diffusion is observed in the second group of crystalline solids, the so-called intercalation compounds. Such compounds are formed by the injection of guest ions from the electrolyte and their charge-compensating electrons into a solid framework. The materials are mixed, ionic, and electronic conductors, so they can be used as electrode material for metal-ion batteries. The different aspects of mineralogical crystallography, composition, and physical properties of these compounds were considered in [10]. The ionic conductivity of certain crystals is now widely used in metal-ion power supplies in the military, medical, household, and industrial electronic devices. The structural types of a number of minerals have been found to be intrinsic to most materials possessing ionic conductivity [11,12]. The aim of this paper is devoted to the structure peculiarities and diffusion mechanism in three types of mineral-like fast ion conductors with the tetrahedral, octahedral, and mixed frameworks.

2. Basic Structural Requirements for Ionic Conductivity

The existence of superionic conductivity depends largely on the structural features of the material. Here are just the basic ones [13]:

1. For ions to be able to move in the unit cell, the number of crystallographic positions energetically close to their sites must be greater than the number of ions themselves.
2. The energy of disorder of ions in the crystal lattice and the energy spent on their movement must be small.
3. The ease with which an ion can move to a neighboring site is controlled by the activation energy. The activation energy is the main factor influencing ionic conductivity.
4. In the crystal structure, the channels for ion motion must have commensurate size with their ionic radii.

The above requirements are satisfied only by special crystals, in the structure of which atoms of one or several varieties partially occupy their positions. This opens up the possibility for their movement under changing external physical and chemical conditions. Materials with high ion mobility are used in many fields of science and technology. It can be said that over the last 40 years, they have changed our world significantly, occupying the most important place in the development of compact current sources and batteries, which were first used in miniature headphones and now in electric vehicles [14].

A few examples which confirm the aforementioned statements are reported below. Synthetic analogs of Na_2TiSiO_5 natisite, a typical mineral of ultraagpaites and hydrothermalites, with the compositions Na_2TiGeO_5 and Li_2TiGeO_5 [15,16] can serve as an illustration of the structural condition of ionic conductivity. The crystal structure of Na_2TiGeO_5 is shown in Figure 1. Perpendicular to the [001] axis, layers of tightly bound Ge-tetrahedra [GeO_4] and square pyramids [TiO_5] are clearly visible. In the space between the layers, mobile Na ions (pink spheres) can move freely. As can be seen in Figure 1b, the conductivity, parallel to the *a*-axis, is 10^3–10^4 times higher compared to the movement of alkali cations along the *c*-axis.

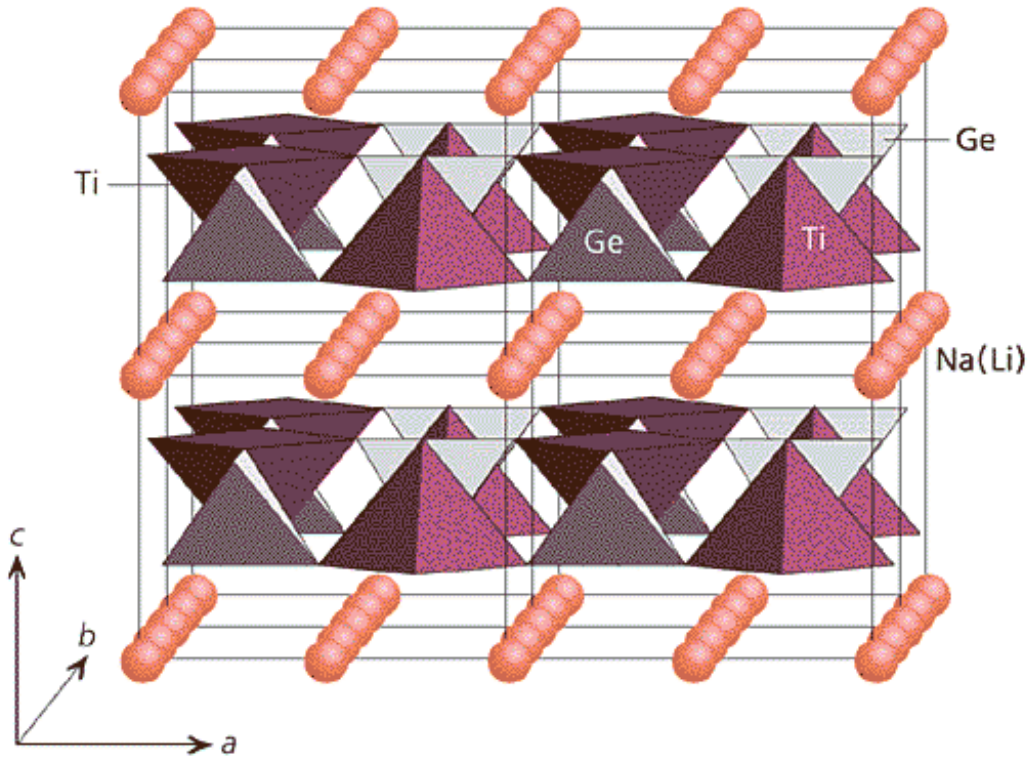

(**a**)

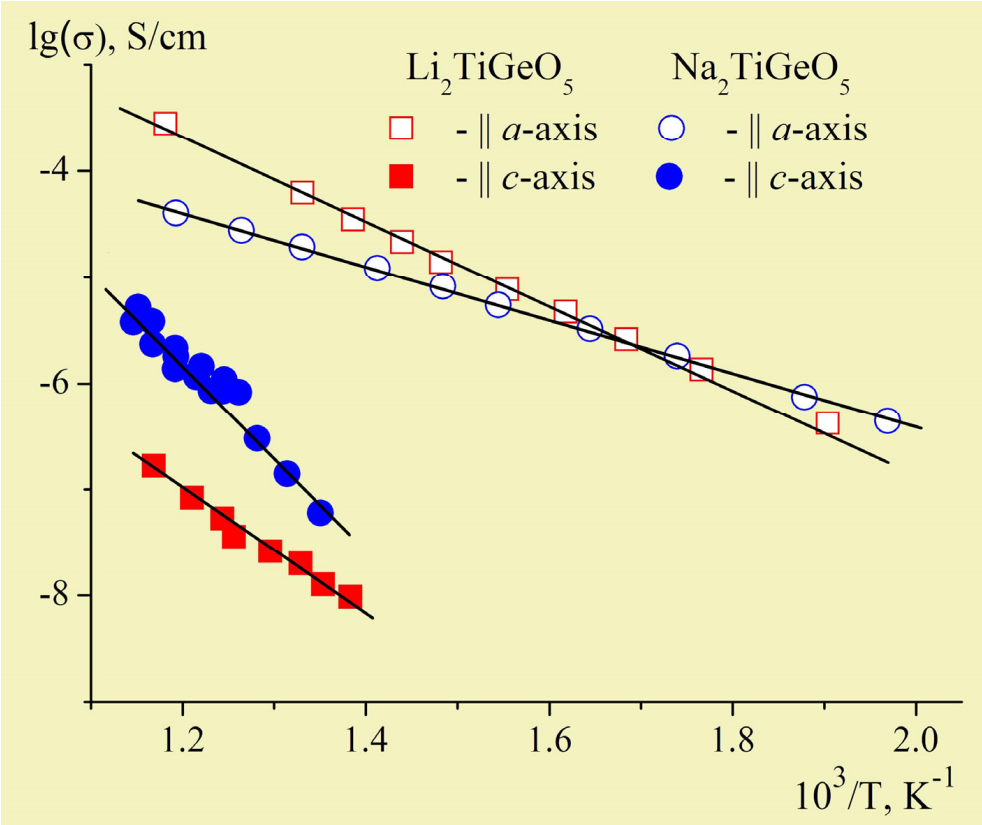

(**b**)

Figure 1. Crystal structure of Na_2TiGeO_5 (**a**), data from [13,16]. The temperature dependence of ionic conductivity related to the movement of alkaline cations within the structures of two natisite analogs—Na_2TiGeO_5 and Li_2TiGeO_5 (**b**).

The pearceite-polybasite group of minerals with general formula $(Ag,Cu)_{16}M_2S_{11}$, where M = Sb and As, can also be considered as a homogeneous series with a fast ion conducting form at high temperature [17,18]. Their structures are described as a regular succession of two module layers stacked along the *c*-axis: a first module layer (labeled A), with general composition $[(Ag,Cu)(As,Sb)_2S_7]^{2-}$, and a second module layer (labeled B), with general composition $[Ag_9CuS_4]^{2+}$ (Figure 2). The observed structural disorder in the B layer is strongly related to the fast ion conduction character exhibited by these minerals. In this module layer, Ag ions can adopt linear to tetrahedral coordination, and they have numerous available sites. Those sites are very close to each other, making a diffusion path in the plane possible (001). Thus, the conductivity in polybasite 222 increases from $5.3{\cdot}10^{-6}$ S/cm at 250 K to $1.8{\cdot}10^{-2}$ S/cm at 385 K. A similar trend is observed in pearceite, where the values of conductivity increase from $4.5{\cdot}10^{-5}$ S/cm to $8.2{\cdot}10^{-3}$ at 250 K and 385 K, respectively [17].

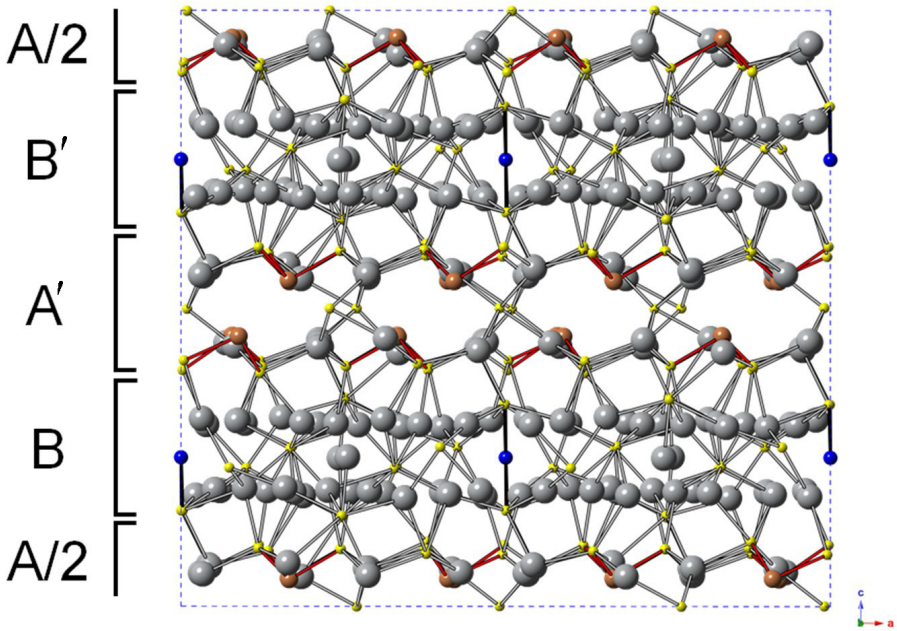

Figure 2. Projection of the polybasite $Ag_{14.88}Cu_{1.22}Sb_2S_{11}$ ordered structure (polytype 222 with doubling of *a*, *b*, and *c* cell dimensions) along [010] with alternation of two-layer modules $[(Ag,Cu)_6Sb_2S_7]^{2-}$ A(A′) and $[Ag_9CuS_4]^{2+}$ B(B′). The modules A′ and B′ are symmetrically equivalent to A and B. Red balls—Ag/Sb, blue—Cu, grey—Ag/Cu, yellow—S.

As shown in Figure 2, there are two individual Ag^+ layers forming a coupled Ag^+ bi-layer hexagonal $[Ag^I{}_9]^{9+}$ sub-structure in these mineral solid electrolyte systems within each B module with $[Cu^IS_4]^{7-}$ slab located in between [19]. The motion of any one Ag^+ ion necessarily impacts the neighboring Ag^+ ions, suggesting that they must somehow move in a distinctly correlated fashion. However, the diffusion of Ag^+ ions results in the mutual incommensurability of the two-component sub-structures. Regarding the use of electron diffraction, two possible modes of incommensurability were discussed: (i) The hexagonal layers with Ag^+ ions should, as far as possible, relate to one another as close-packed layers; (ii) To maintain physically reasonable separation distances between Ag^+ layers across the bi-layer is to slightly displace them along the *c*-direction, a feature that was seen in the average structure refinement [18,19].

Another extremely interesting example of a direct connection between structural features and ionic conductivity is the $Na_5YSi_4O_{12}$ crystal. The characteristic features of this structure are 12-membered (Si,O)-rings of silicon-oxygen tetrahedra (Figure 3) [20].

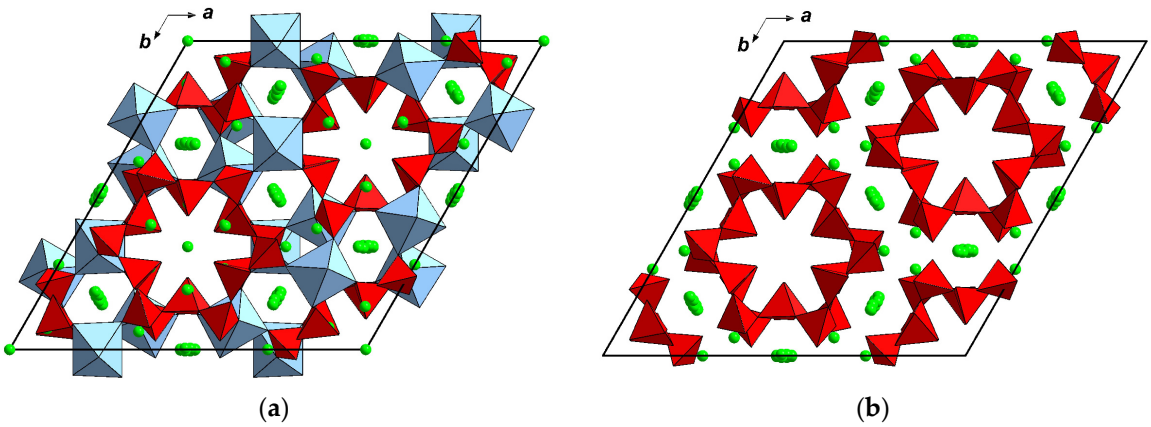

Figure 3. Structure of $Na_5YSi_4O_{12}$: Projection of the framework of silicon-oxygen rings Si_4O_{12} (red color) and octahedra YO_6 (blue color) located at different levels. The positions of Na atoms are indicated by balls in green color (**a**). The same projection (001) with all positions of Na atoms highlighted (green color) in the spaces between the 12-membered providing ionic transport within the mixed framework (**b**). The figures are plotted using the coordinates of atoms from [21].

No one at that time paid attention to another feature of this structure. According to the symmetry of the cell, it should contain 90 Na atoms. However, regarding the occupancy of the found positions, only 48 atoms were localized. Later, in 1978, a group of researchers led by R.D. Shannon suggested [22] that this discrepancy should be associated with the possible movement of Na atoms within the structure, i.e., with ionic conductivity. The positions of these mobile Na atoms are shown in Figure 3b. As a result, it turned out that static Na atoms are located inside the (Si,O)-rings, while mobile ones are located between the columns formed by them inside the channels, the width of which is determined by the size of the octahedra of rare-earth cations. Furthermore, it was shown that the conductivity increases with increasing radius of R^{3+} cation, as well as with increasing temperature (Figure 4).

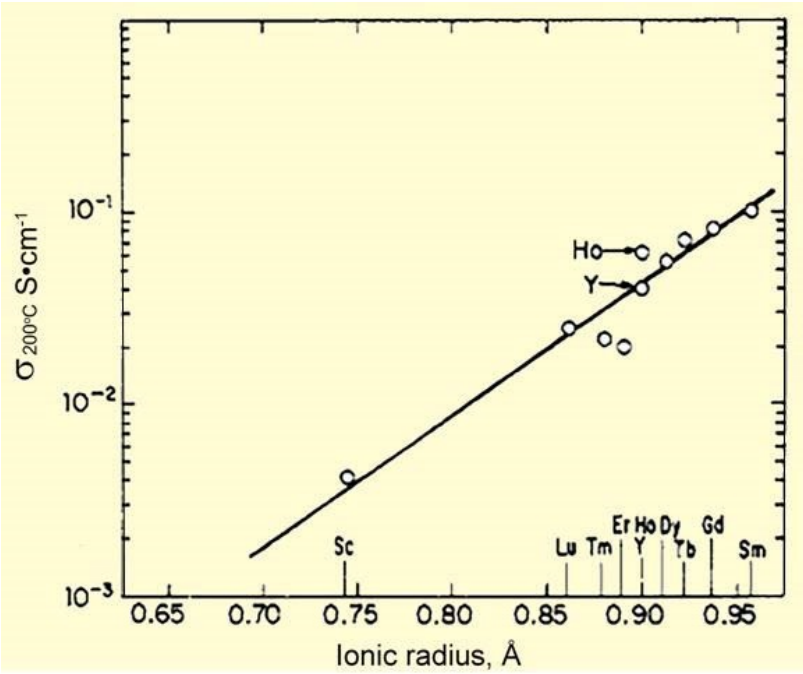

Figure 4. Increase of conductivity in crystals of $Na_5TRSi_4O_{12}$ series with increasing radius of rare-earth (TR) cation, adapted from [22].

At the same time, in $Na_5MSi_4O_{12}$ crystals, where M = TR, Fe, In, Sc, Y, the high values of conductivity were obtained. They range from $2{\cdot}10^{-3}$ S·cm^{-1} in $Na_5ScSi_4O_{12}$ (r Sc = 0.885 Å) to $3{\cdot}10^{-1}$ S·cm^{-1} in $Na_5SmSi_4O_{12}$ (r Sm = 0.958 Å) at 300 °C.

The results obtained using X-ray diffraction methods are extremely important for understanding the structural requirements of ionic conductivity in crystals. The structure of $K_3NdSi_6O_{15}$, determined in 1977 [23] (Figure 5), confirms this statement.

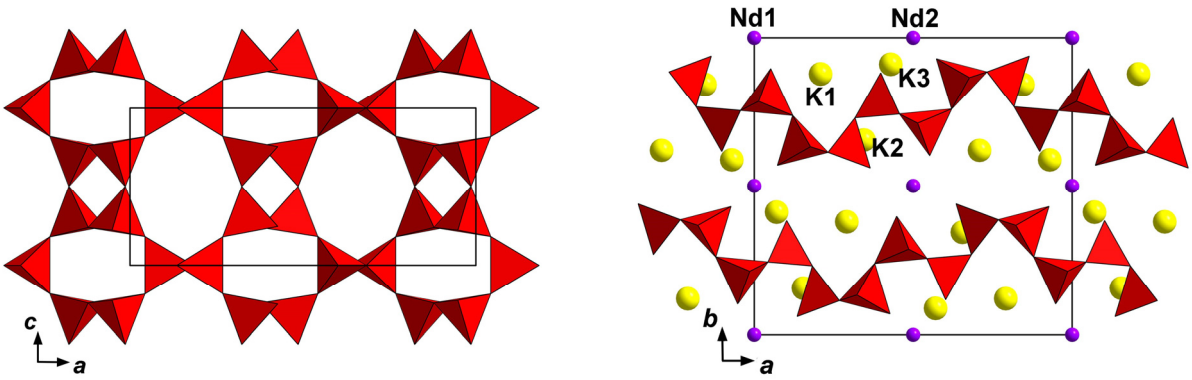

(**a**) (**b**)

Figure 5. Structure of $K_3NdSi_6O_{15}$: dimeta-silicate layer [Si_6O_{15}] (010) (**a**); projection on the (001) (**b**) plane.

The first result of this work was the discovery of the original dimeta-silicate layer [Si_6O_{15}] containing four-, six- and eight-membered silicon-oxygen rings, similar to those found in rare mineral dalyite $K_2ZrSi_6O_{15}$ [24]. At the same time, rather high values of isotropic thermal parameters of alkali K^+ cations in the range of 3.90–5.46 Å^2 did not provoke a special interest.

After 16 years, this very circumstance allowed the authors of [25] to conclude that this material, based on structural considerations, was a likely fast ion conductor. All features of this interesting structure were confirmed, but its refinement in the anisotropic approximation [25] allowed to establish that K1 thermal displacement along one of the three coordinate axes was twice as large as the other two ($\times 10^{-2}$) Å^2: $U11$ = 5.9, $U22$ = 5.4, $U33$ = 10.4. The projection of this structure along [001] clearly indicates the presence of channels in which K1 cations are located and which are considered as probable directions for ionic conduction. Accordingly, K1 cations are most mobile along [001], which is confirmed by the values of the principal elements of the specific electrical conductivity tensor (10^5 S·cm^{-1}) at 600 °C [26] σ11 = 3.4, σ22 = 6.9, σ33 = 17. Thus, the above-mentioned examples indicate the main crystallochemical criteria inherent in ion-conducting crystals.

3. Ion-Conducting Materials with Tetrahedral Framework of Zincite-Wurzite Type. Li_3PO_4-Polymorphs and Their Relationship with Mineral Lithiophosphate Li_3PO_4

Despite its simple composition, the structural chemistry of the compound Li_3PO_4 is quite complex. It forms three modifications—α, β, and γ [27,28]. The transformation of the β-modification into the higher-temperature γ-form occurs at 500 °C. Further γ-modification at 1170 °C is transformed into α-phase, which then experiences melting at 1220 °C. Thus, α-Li_3PO_4 is stable in a very narrow temperature range.

The main difference between the structures of β-Li_3PO_4 and γ-Li_3PO_4 is presented in Figure 6. In the structure of β-Li_3PO_4 with space group $Pmn2_1$ (structural type of zincite ZnO and wurtzite ZnS), all tetrahedra are oriented equally, whereas in the γ-modification (space group *Pmnb*), both types of tetrahedra have opposite orientation along [001]. This is the reason why the tetrahedra in the γ-Li_3PO_4 structure are interconnected not only by vertices but also by edges (Figure 6b), and the unit cell parameter *b* doubles with respect to β-Li_3PO_4. Lithiophosphate (Li_3PO_4, space group $Pmn2_1$) can be supposed to be a natural form of low-temperature β-lithium orthophosphate. Besides the same space group both

phases have similar cell dimensions. However, their similarity must be validated by the results of the structural study of litiophosphate. Because of the reversibility of the $\gamma \rightarrow \alpha$ transition, attempts to fix α-Li_3PO_4 by quenching have not been successful. Therefore, the question of its structure remains open.

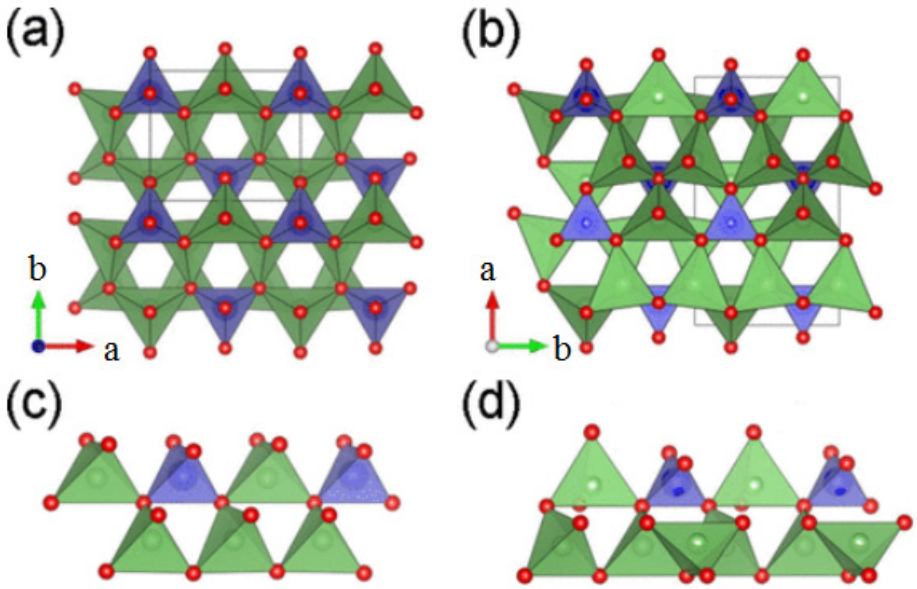

Figure 6. Structures of (**a**) β-Li_3PO_4 and (**b**) γ-Li_3PO_4, with details of polyhedral connectivity shown in (**c**,**d**), respectively. Blue and green—P- and Li-tetrahedra, respectively (adapted from [29]). Red balls—oxygen atoms.

Lower valent cation substitution of P in Li_3PO_4 by Si or Ge requires charge balance through the introduction of additional Li^+-ions, which are located in the interstitial octahedral sites. These derivative compounds, Li_4SiO_4 and Li_4GeO_4, have high ionic conductivity due to the peculiarity of their tetrahedral framework structures. The closest hexagonal package of anions O^{2-} is in their basis. Li^+ ion has a small radius of 0.59 Å, which allows it to move in the relatively narrow voids of crystal structures. The choice of lithium as a charge carrier is also based on its other properties. Lithium is the lightest metal: it is twice as light as water! Its density of 0.534 g/cm^3 is about the same as that of wood [30]. Thus, its properties, charge, high electrochemical potential, and ability to move easily in crystal structures are associated with the use of this element in lithium-ion batteries, which provide the highest gravimetric and volumetric energy densities. Therefore, the isomorphic replacements within the γ-Li_3PO_4 structure type are the focus of many research works, and the corresponding group of compounds is named LISICON (Some authors incorporate into LISICON group all materials with Li-conductivity but not only those with tetrahedral frameworks). For example, substitutions of Si^{4+} and Li^+ ions in Li_4SiO_4 with other cations such as Ge^{4+}, P^{5+}, or Zn^{2+} could lead to significant improvement in conductivity, and $Li_{14}ZnGe_4O_{16}$ has the highest value of about 10^{-1} S·cm^{-1} at 300 °C.

In lithium superionic conductors (LISICONs) with γ-Li_3PO_4-type structure, Li atoms occupy two non-equivalent positions. However, in crystals with multivalent cations isomorphically substituting P^{5+} in tetrahedra, such as $Li_{3.68}(Ge_{0.6}V_{0.36}Ga_{0.04})O_4$ [31], Li-sites are split, and a degree of disorder of Li^+ cations increases. Consequently, they can move more easily within the structure, and the conductivity increases by an order of magnitude.

In total, there are 6 Li positions in the above-mentioned structure (Figure 7a). Two of them with small occupancy are near the two main ones, and the other two are located in channels, acquiring an octahedral coordination that is too large for them. Thus, $Li_{3.68}(Ge_{0.6}V_{0.36}Ga_{0.04})O_4$ exhibited the highest ionic conductivity (1.5×10^{-4} S·cm^{-1}) at 298 K, with extremely low activation energy (~0.26 eV).

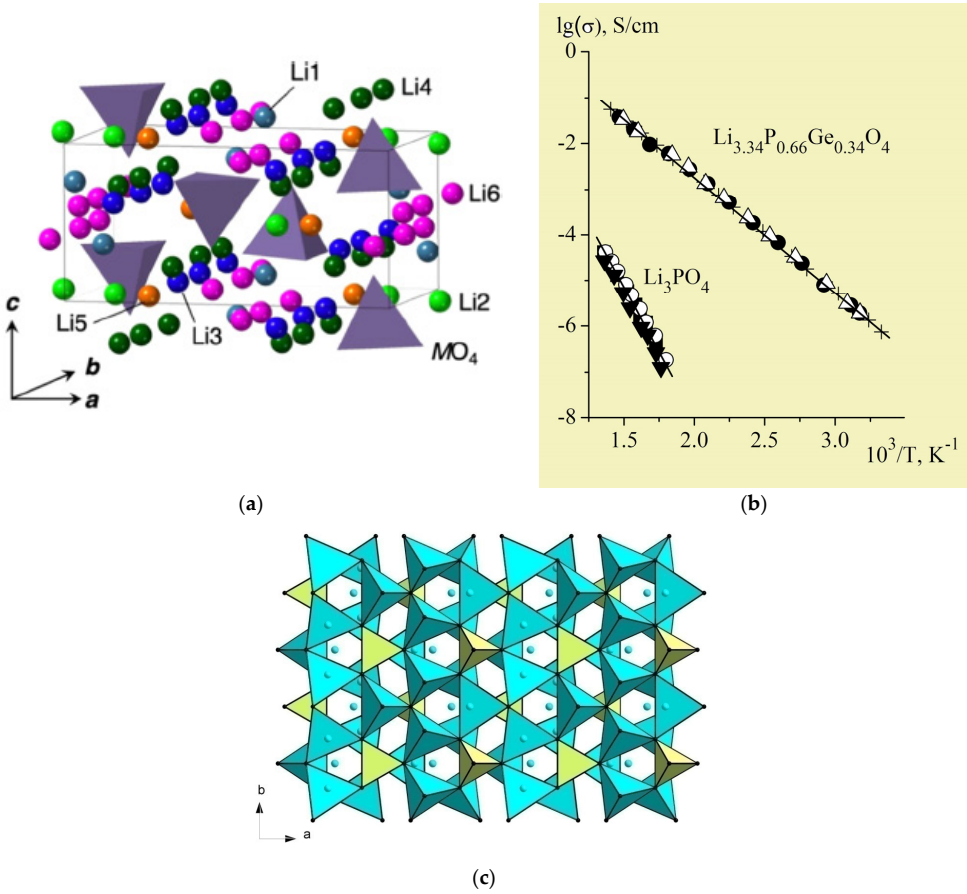

Figure 7. Structural type of γ-Li_3MPO_4 (M—P, Ge, V, Ga, Mo): [PO_4]-tetrahedra marked with grey-violet color, adapted from [31] (**a**). Temperature dependence of ionic conductivity for single crystals Li_3PO_4 and $Li_{3+x}P_{1-x}Ge_xO_4$ (**b**). Different icons represent conductivity values in different crystallographic directions. $Li_{3.17}(P_{0.69}Ge_{0.24}Mo_{0.07})O_4$ tetrahedral framework with one additional Li position indicated by a green circle in the structural channel (**c**). LiO_4 and PO_4 tetrahedra are shown with green and yellow colors, respectively.

In the superionic conductor $Li_{3+x}P_{1-x}Ge_xO_4$ (x = 0.34), two basic Li sites are partially filled with occupancies 0.85 and 0.83. In addition to these, there are four positions of Li cations with relatively low occupancies. Two of these Li^+ cations are located near the main positions at distances of 0.86 and 0.81 Å, respectively, whereas two other Li atoms occupy octahedral cavities in the framework. Evidently, these cavities are too large for small Li cations. One of them has a large value of the atomic displacement parameter, and another one shows the replacement of octahedral coordination by a pseudo-tetragonal pyramidal one [32]. In this compound, all six Li atoms have population coefficients less than unity, which opens the possibility for their transport, determining high cationic conductivity (Figure 7b) with an increase in temperature. The values of specific conductivity for $Li_{3.34}P_{0.66}Ge_{0.34}O_4$ are $1.8 \cdot 10^{-6}$ and $3.7 \cdot 10^{-2}$ $S \cdot cm^{-1}$ at 40° and 400 °C, respectively [32].

The number of additional Li positions depends on the variety of cations substituting for P. In the structure $Li_{3.17}(P_{0.69}Ge_{0.24}Mo_{0.07})O_4$ [32], due to the presence of highly covalent Mo as an isomorphic impurity, the Li content decreases, and the number of positions occupied by it decreases to 5 in the γ-Li_3PO_4-type structure (Figure 7c).

The similarity of the structure of γ-Li_3PO_4 with mineral-like electrode materials for metal-ion batteries of the triphylite $LiFePO_4$ group was noted in [33]. Both structures contain hexagonal closest packing of O^{2-} anions, and in both cases, phosphorus atoms occupy 1/8 of the tetrahedral voids (Figure 8) with their very close spatial arrangement.

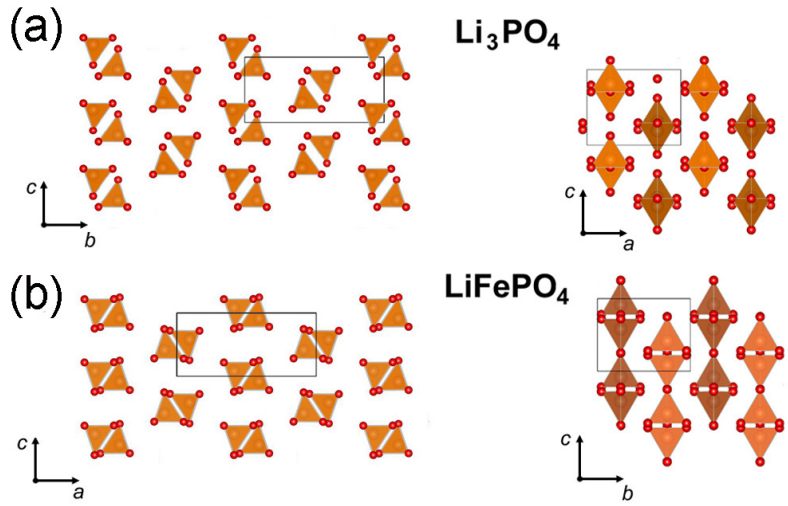

Figure 8. Geometrically close positions of [PO_4] tetrahedrons in Li_3PO_4 (**a**) and $LiFePO_4$ (**b**) structures, reprinted with permission from [33].

It is no coincidence that Li_3PO_4 was used as a template at the final stage of the multistep synthesis of $LiFePO_4$ [33]. Thus, taking into account the structural similarity of both compounds, the formalized reaction scheme allows isomorphic substitution of 2 Li in Li_3PO_4 for 1 Fe in $LiFePO_4$.

4. Ion-Conducting Materials with Octahedral Ilmenite-like Framework

The structure of a synthetic analog of brizzite $NaSbO_3$ (Figure 9) with the structural type of ilmenite also shows a number of features characteristic of ion-conducting crystals [34].

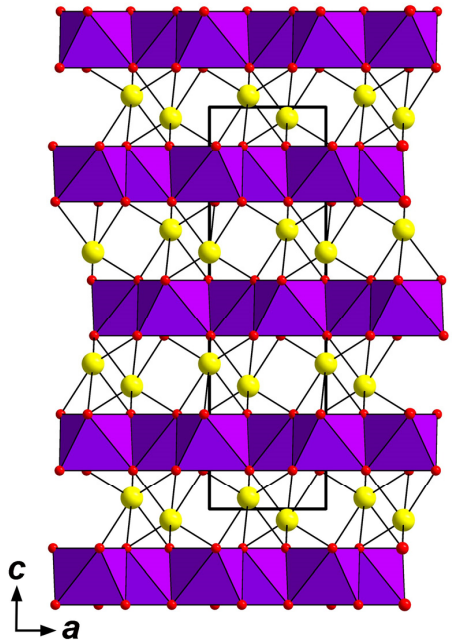

Figure 9. Structure of $NaSbO_3$ brizzite. SbO_6-octahedra (violet color) form gibbsite-like layers (001). Na atoms (yellow spheres) are located in the interlayer space. Plotted using coordinates of atoms from [35]. Red balls—oxygen atoms; solid line marks the unit cell.

Synthetic $NaSbO_3$ crystals form four polymorphic forms. Initially, a cubic modification with space group *Pn*3 became known [36]. Another cubic polymorphic form of $NaSbO_3$, but with sp. gr. *Im*3 and with a disordered arrangement of Na atoms in the unit cell, became

known almost 35 years later [37]. This metastable compound was synthesized at a pressure of 2 GPa on the basis of ion exchange involving cubic modification of $KSbO_3$ (sp. gr. *Im*3) in $NaNO_3$ melt. The detailed analysis of the rhombohedral ilmenite-like modification of $NaSbO_3$ with space group *R-3* was reported in [34]. The lower ionic conductivity of this ilmenite-like phase $NaSbO_3$ (3.0×10^{-5} S·cm^{-1} at 400 °C) in comparison with that of the metastable cubic $NaSbO_3$ (5.6×10^{-2} S·cm^{-1} at 300 °C) has been attributed to its structural low dimensionality, strong Na^+–oxygen bond, and high sodium occupancy factor [34]. Later on, considering that the structural characteristics, physical properties, and consequently the potential applications of $NaSbO_3$ compound in the industry depend on the synthesis method and reaction conditions, its rhombohedral crystals were obtained at temperatures lower than 750 °C [38]. This symmetry is also characteristic of the mineral brizzite [35]. Besides these phases, an orthorhombic form of $NaSbO_3$ with a distorted perovskite-like structure and with the space group *Pnma* is known [39].

The structures of both cubic modifications contain a framework of SbO_6 octahedra. Pairs of such octahedra are connected along the common edge form [Sb_2O_{10}] dimers, which are linked to each other along the vertices (Figure 10). Inside the octahedral framework, tunnels are formed along [111], which intersect at the vertices and in the center of the unit cell. In these tunnels, Na atoms are localized either with an ordered arrangement in two non-equivalent positions in sp. gr. *Pn*3 or with partial occupancy of the two main positions in sp. gr. *Im*3 (the corresponding occupancy coefficients are 0.82 and 0.29).

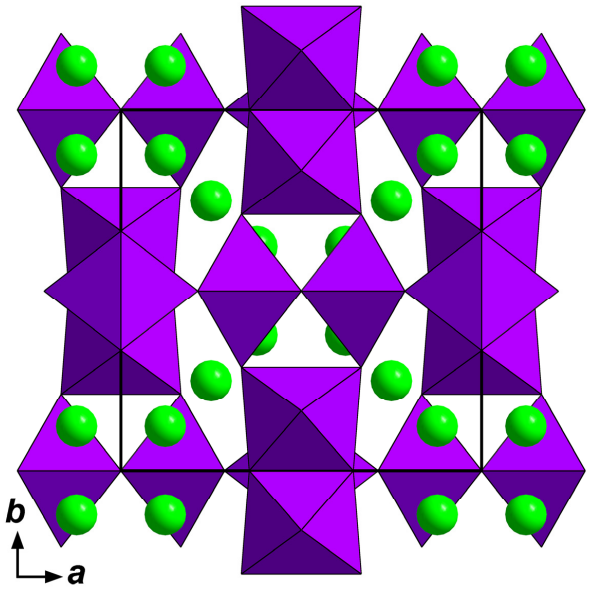

Figure 10. Octahedral [SbO_3] framework (purple color) in the structures of cubic modifications of $NaSbO_3$. Green balls are Na atoms. Plotted according to the coordinates from [37].

Similarly to ilmenite, gibbsite layers of edge-bound Sb-octahedra and more distorted Na-octahedra alternate in the structure of the rhombohedral modification of $NaSbO_3$ along [001] [34]. The data obtained on structural modifications of $NaSbO_3$ polymorphs allow to understand [34] the difference of ion-conducting properties of the cubic phase (*Im*3) and rhombohedral phase with the structural type of ilmenite. It was noted above that the rhombohedral polymorph exhibits a lower value of conductivity. Additionally, its activation energy is higher: 0.66 eV vs. 0.29 eV in the metastable cubic phase.

In the structure of cubic polymorph (*Im*3), Na atoms are disordered in two positions inside the 3-dimensional system of intersecting tunnels. In rhombohedral $NaSbO_3$ with ilmenite structure type, these atoms are ordered in octahedral positions between layers of SbO_6 octahedra. Therefore, the Na^+ motion in the former case occurs along 3D axes, whereas in the latter case, it is restricted to 2 dimensions.

In the ilmenite-like structure, the average Na-O distance of 2.424 Å is significantly shorter compared to the cubic phase, where it is 2.70 Å. Accordingly, this difference leads to reduced conductivity in the rhombohedral polymorph. On the contrary, the Na-Na distance of the cubic structure is 2.30 Å, while in the rhombohedral structure, it is 3.175 Å. These values should affect the difference in the reduced activation energy: 0.66 eV for rhombohedral ilmenite-like crystals vs. 0.29 eV for the cubic phase. Another factor that has a significant influence on ionic conductivity is determined by the difference in the degree of occupancy of Na^+ cations in their positions. In the cubic structure, these values are equal to 0.82 and 0.29, and in the rhombohedral structure, the occupancy coefficients of Na^+ cations are equal to 1.

Finally, the transport of Na^+ cations should be affected by the size of conductive channels. According to [40], their optimal width for Na^+ cations should be 4.58 Å. In the cubic structure, it exceeds 5.0 Å, and this partly determines the low value of the activation energy of 0.29 eV. In ilmenite-like $NaSbO_3$, the diffusion of Na^+ cations occurs inside the layers. The width of their conductive pathways is reduced to the smaller distance of 4.568 Å between the nearest two O atoms. Consequently, it should lead to an increase in the activation energy value of 0.66 eV.

In the phase with a body-centered unit cell, even the 6 shortest Na-O 2.65 Å distances in Na-octahedra exceed the sum of ionic radii, which should also contribute to the mobility of Na^+ cations. According to [37], the mobility of Na^+ cations in $NaSbO_3$ and in superionic crystals of β-aluminum oxide $Na_2O{\cdot}11Al_2O_3$ (conductivity is of the order of 10^{-2} $S{\cdot}cm^{-1}$) must have common prerequisites. First of all, it should be recalled that the structure of β-aluminum oxide, as well as its composition, is very different from that of α-Al_2O_3 corundum. The structure of β-aluminum oxide (sp. gr. $P6_3/mmc$) contains mirror-bound spinel-like blocks of Al-tetrahedra and Al-octahedra. The ion-conducting layers with Na^+ cations are located between them (Figure 11). In this phase, Na^+ cations cross an edge common to the two octahedra during their movement, whereas in the $NaSbO_3$ structure, they pass through a face common to the neighboring octahedra [37]. However, both compounds have close values of ionic conductivity.

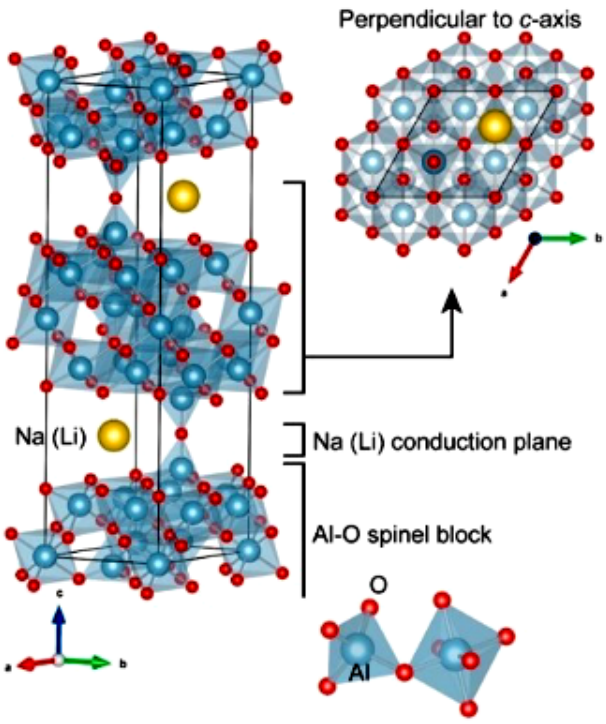

Figure 11. Structure of β-aluminum oxide. Two neighboring spinel blocks are connected by a weakly populated, conducting layer in which Na^+ cations are located, adapted from [41].

The β-alumina compounds with mono-valent cations, like sodium or potassium, have no stoichiometric composition, and their disordered structures are known as fast ion conductors. This peculiarity makes them attractive for energy storage applications [42]. The β-alumina presents the great advantage of being a very stable host lattice. It is separated into two species, namely, hexagonal β-alumina and rhombohedral β″-alumina types [43]. The incorporation of Li in sodium β-alumina by laser chemical vapor deposition (CVD) was reported in [41].

The structure of β-alumina exhibits the Frenkel defects. This type of defect forms when Al leaves its place in the structure, creating a vacancy and becoming an interstitial by lodging in a nearby location. The ionic conductivity depends on the correlations between the compensating defects and the diffusing ions. With the use of diffuse scattering measurements, the formation of Al Frenkel defects, which lock the extra bridging oxygen ions in the diffusing plane of β-alumina, was considered in [44]. Rods of diffuse scattering were observed in β-alumina grown from the flux with Ag, K, Rb, and Eu substituted for Na in the diffusing plane. They result from a strong interaction among the diffusing ions within a conducting layer and a weak correlation between layers. Consequently, three types of superstructure unit cells agree with observed XRD data for isomorphic varieties of β-alumina: (i) Those containing one diffusing ion; (ii) Those with two diffusing ions; (iii) Those with two ions plus one extra bridge oxygen.

It is worth noting that, to date, only two minerals with structures of the β-alumina type are known: kahlenbergite $KAl_{11}O_{17}$ and diaoyudaoite $NaAl_{11}O_{17}$ [45]. The structure of kahlenbergite is shown in Figure 12.

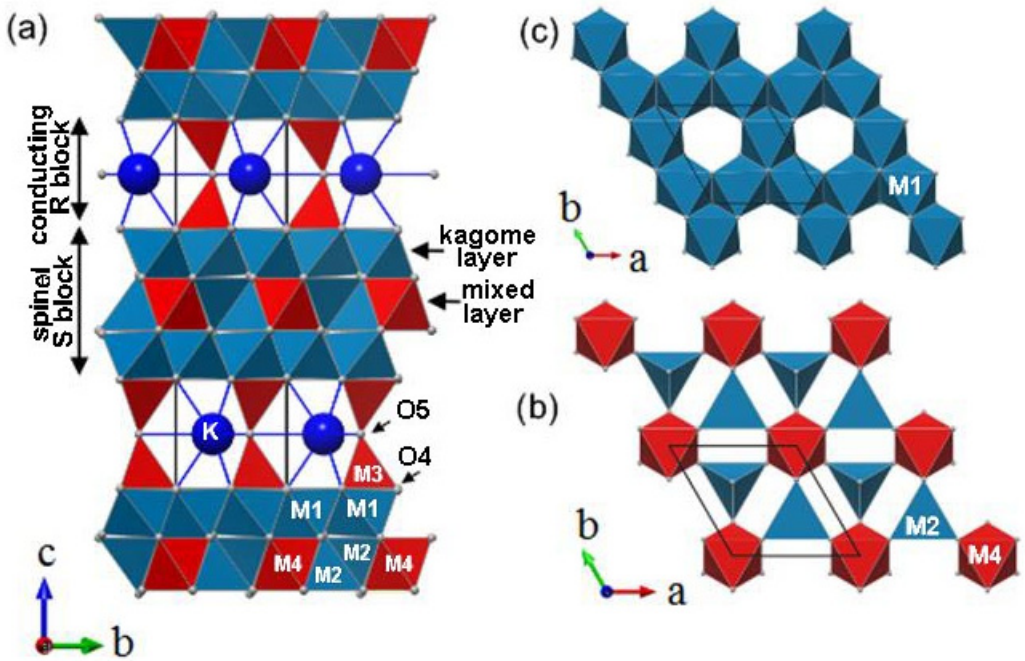

Figure 12. Structure of kahlenbergite. (**a**) Unit cell is made of two spinel (S) blocks and two conducting R blocks. Spinel blocks can be divided along *c* into mixed layers (**b**) and kagome layers (**c**). In mixed spinel (S)-layers AlO_6 octahedra (M4) and $(Al_{0.56}Fe_{0.44})O_4$ tetrahedra (M2) share the corners. The kagome layer is built by edge-sharing $(Al_{0.92}Fe_{0.08})O_6$ octahedra (M1), adapted from [45].

5. Mixed Frameworks in Natural and Synthetic Ionic Conducting Crystals with NASICON Structure Type

The discovery of fast-ionic conductivity in β-alumina stimulated interest in using solid electrolytes in thermoelectric generators, which convert heat into electrical energy. The ionic mobility in the layered structure of β-alumina occurs in two dimensions. Therefore, the framework structures with possible ionic transport in three dimensions attracted special attention [46,47].

Among the most promising compounds from the point of view of ionic conductivity, the representatives of the NASICON family with the general formula $Na_{1+x}Zr_2Si_xP_{3-x}O_{12}$, $0 < x < 3$ occupy an important place. It was their composition that determined the name of the whole NASICON family: NA—from Na, SI—from super ionic, and CON—from the conductor. The study of its representatives began in 1976 when the prototype of NASICON, $Na_{1+x}Zr_2Si_xP_{3-x}O_{12}$, was reported [46,47]. The ionic conductivity of this solid solution at 300 °C achieved a high value of 0.2 $S{\cdot}cm^{-1}$ with low activation energy 0.29 eV when x = 2 [47]. These values are comparable to Na-β-alumina above 443 K.

Later, the class of these materials expanded, and now it includes a wider set of compounds, such as $AM_2(TO_4)_3$, where A = Li, Na, K; M = Zr, Th, Fe, Sc, etc.; and T = P, As, Si, S, Se, etc., which are characterized by high cation mobility at relatively low temperatures and should have high hydrolytic and thermal stability. The data on the structure and ionic conductivity of NASICONs are discussed in an enormous number of papers [48]. Here, only some aspects of their correlation are considered.

The most specific feature of NASICON structure type is a mixed framework with the rhombohedral (*R*-3*c*) symmetry which is formed by corner-sharing metal octahedra and oxo-tetrahedra, as illustrated in Figure 13a.

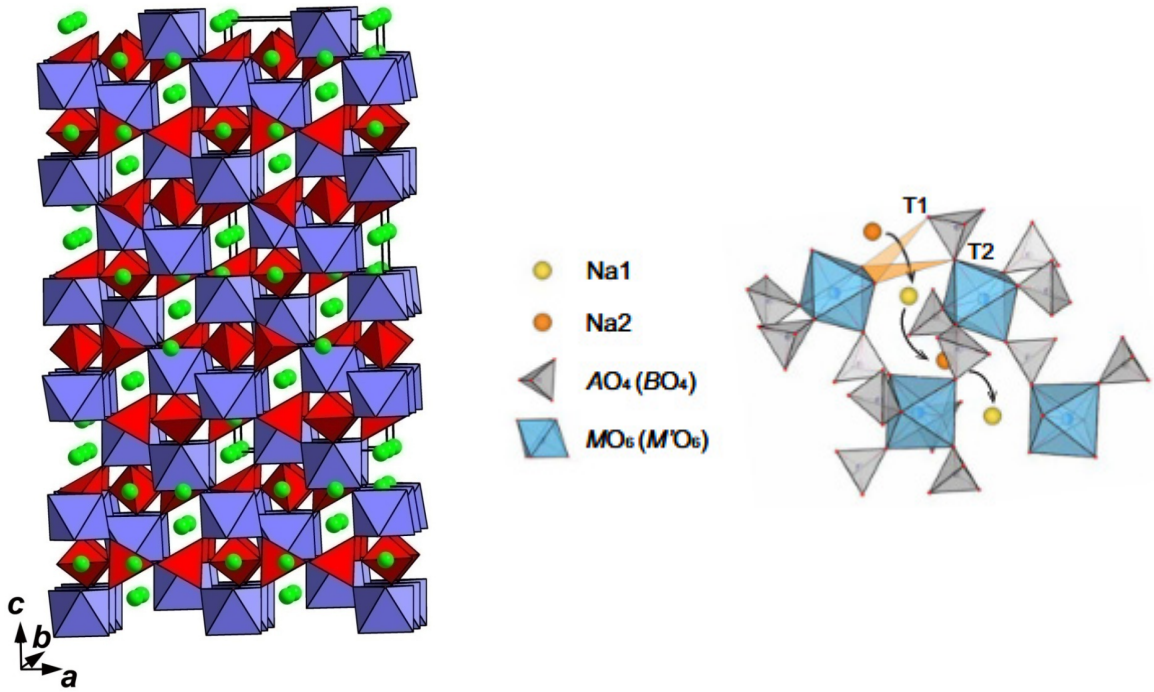

(**a**) (**b**)

Figure 13. NASICON mixed framework. Green spheres are Na atoms, Zr-octahedra and (Si,P)-tetrahedra are shown with purple and red colors, respectively (**a**). The sites of Na1 and Na2 atoms within the mixed framework and the paths of their migration (**b**), adapted from [48].

All oxygen atoms are bridging, i.e., they are involved in sharing the links between polyhedra. Thus, each octahedron is connected to six tetrahedra and each tetrahedron—to four octahedra. Na^+ ions occupy two positions: Na(1) ions are located in distorted $[NaO_6]$-octahedra and Na(2) ions lie in framework voids formed by 10 oxygen atoms. Na ions can migrate from one site to another through two triangular bottlenecks. Their transport determines the fast ion conductivity of the NASICON crystal and is shown in Figure 13b.

NASICON compounds can also form in a monoclinic symmetry (*C*2/*c*) depending on the composition and temperature, which splits the Na2 site into two different sites. However, the skeleton remains the same, and thus, the ion transport within the framework channel is similar [48].

The split of Na2-positions into three sites in monoclinic modification of NASICON-type structure $Na_3FeV(PO_4)_3$, which leads to the doubling of unit cell volume [49], is shown in Figure 14a in comparison with the chemically related rhombohedral structure of $Na_4FeV(PO_4)_3$ with almost fully occupied two Na-sites (Figure 14b).

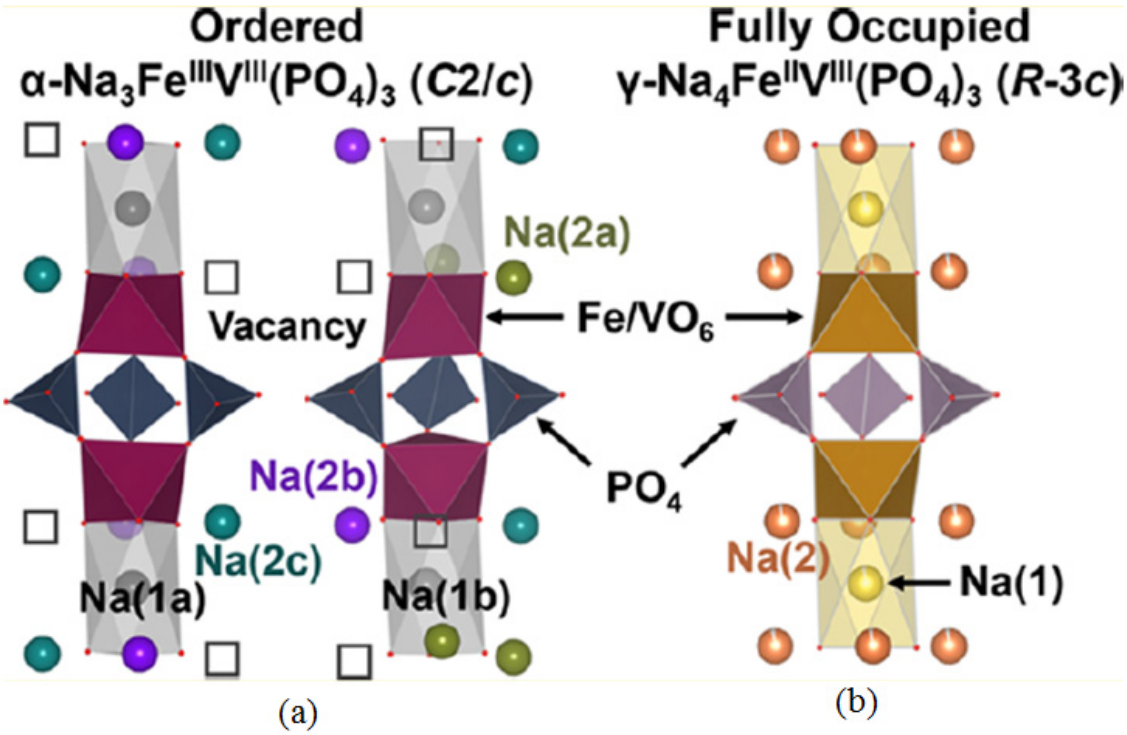

Figure 14. Schematic representations of Na^+ distributions in $Na_3FeV(PO_4)_3$ (**a**) and $Na_4FeV(PO_4)$ (**b**), reprinted with permission from [49].

The correlation between conductivity and composition of NASICON compounds was carefully analyzed in [48]. In general, the ionic conductivity increases as the silicate content increases in mixed SiO_4/PO_4 NASICON compounds [48]. In particular, the total conductivities of NASICON crystals with the pure phosphate group are in the range of 10^{-6} to 10^{-5} S·cm^{-1}, whereas those of phases with the $(SiO_4)(PO_4)_2$ groups are in the range of 10^{-5} to 10^{-4} S·cm^{-1}. The highest values of ionic conductivity of 4.4×10^{-4} S·cm^{-1} at room temperature (~25 °C) were achieved in $Na_3HfZr(SiO_4)_2(PO_4)$ [48] and 1.65×10^{-1} S·cm^{-1} at 473 K in $Na_{3.4}Zr_2Si_{2.4}P_{0.6}O_{12}$ [50]. Within each polyanion group, the ionic conductivity shows a non-monotonic trend with an average radius <r M> of M-cations. Indeed, the ionic conductivity increases with <r M> only up to an optimal value. For example, the ionic conductivity increases from 2.40×10^{-6} to 6.48×10^{-5} S·cm^{-1} in going from $Na_3HfMg(PO_4)_3$ (<r M> = 0.715 Å) to $Na_3ScIn(PO_4)_3$ (<r M> = 0.773 Å) and from 6.17×10^{-5} S·cm^{-1} for $Na_3Hf_{1.5}Mg_{0.5}(SiO_4)(PO_4)_2$ (<r M> = 0.713 Å) to 1.87×10^{-4} S·cm^{-1} for $Na_3HfSc(SiO_4)(PO_4)_2$ (<r M> = 0.728 Å).

The conductivity of the solid solution $Na_{1+x}Zr_2Si_xP_{3-x}O_{12}$ correlates with the following limits on x values: $1.8 < x < 2.4$. At smaller values of x, there will be few Na^+ cations (charge carriers) in the structure and a correspondingly smaller conductivity of the crystal. At larger values of $x > 2.4$, all possible positions for Na^+ will be occupied, and they will not be able to move along the transport pathways.

According to [51], one of the representatives of NASICON—$LiZr_2(PO_4)_3$ has a linear dependence of conductivity on temperature (Figure 15), which is typical for many above considered fast ion conductors.

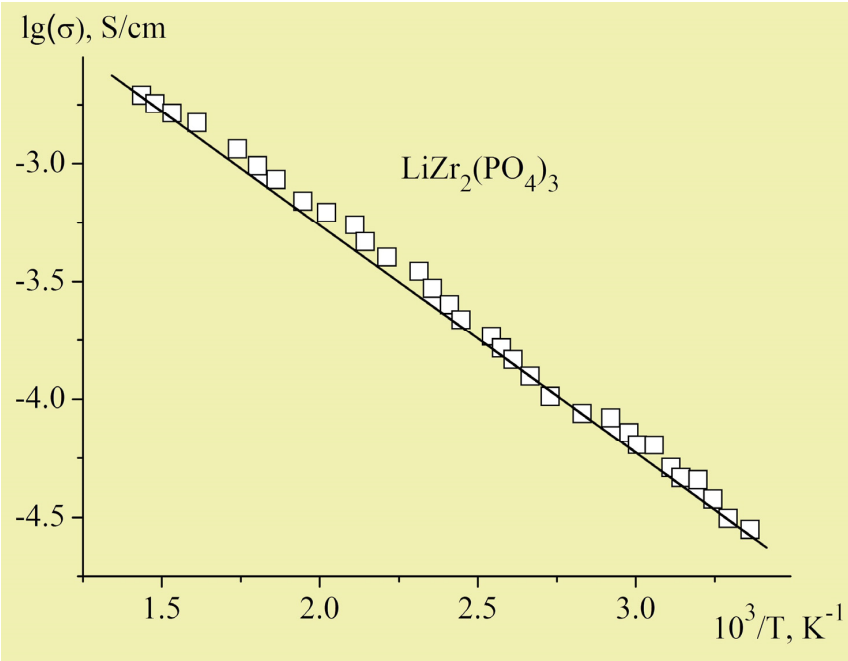

Figure 15. Increase in conductivity with increasing temperature in $LiZr_2(PO_4)_3$ crystals with NASICON-type structure, adapted and modified from [51]. □—experimental points.

A natural analog of the NASICON family compounds is kosnarite $KZr_2(PO_4)_3$ [52]. Its rombohedral (space group *R*-3c) structure (Figure 16), like other representatives of NASICON, contains a mixed framework $[Zr_2P_3O_{12}]$. K atoms are located in the centers of antiprisms on the inversion axes -3 in its cavities. In addition to K mobility, kosnarite possesses ion-exchange properties, accumulating actinide atoms [53].

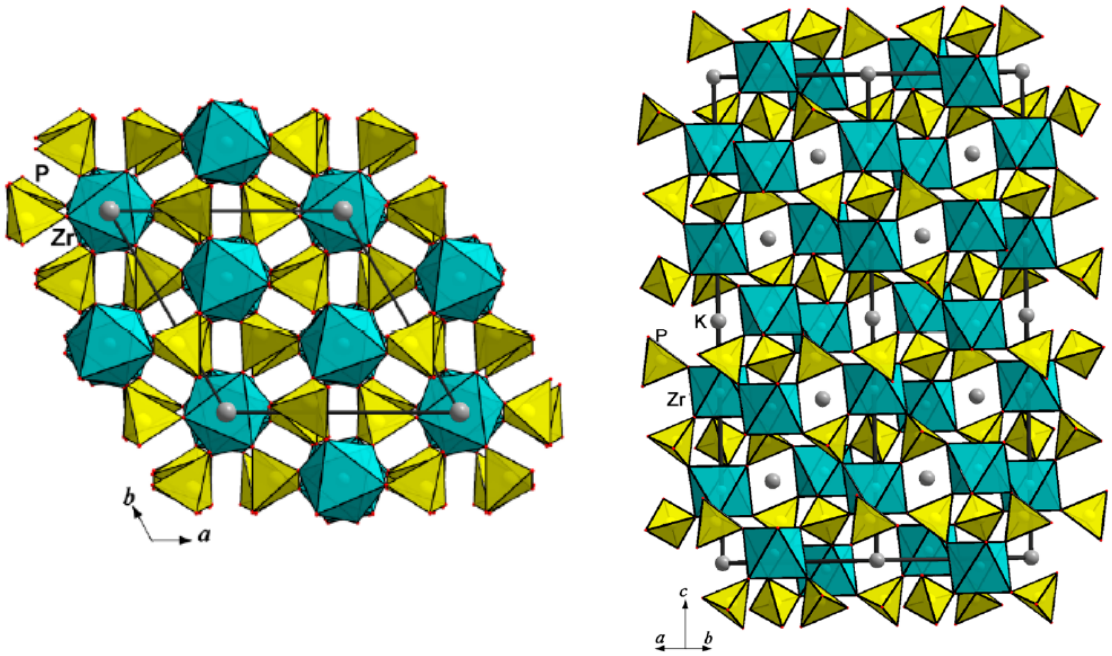

(**a**) (**b**)

Figure 16. Structure of kosnarite $KZr_2(PO_4)_3$ in projection (001) (**a**) and along [110] (**b**), adapted from [11].

6. Ion Transport in the Structures of Conducting Crystals

Li^+ superionic conductors are highly desirable for solid-state lithium batteries. However, only a few crystalline Li^+ compounds are characterized by high ionic conductivity, particularly at room temperature. Among the materials exhibiting high ionic conductivity with relatively low transition temperatures to the superionic state, lithium-ion conductors with general formula $Li_3M_2(PO_4)_3$ (M = Fe, Sc, Cr, In) and with mixed framework structures are very promising. The three-dimensional framework of the $Li_3Sc_2(PO_4)_3$ structure is built of $[ScO_6]$ octahedra and $[PO_4]$ tetrahedra connected through common oxygen vertices (Figure 17). Three non-equivalent Li^+ ions are located in the channels of this framework [54].

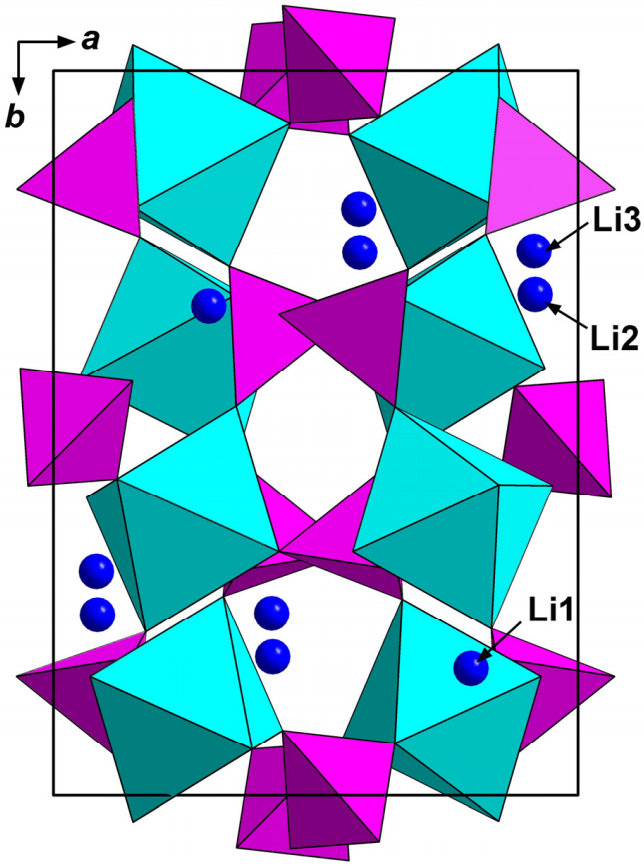

Figure 17. The structure type $Li_3M_2[PO_4]_3$ (M = Sc, Fe): blue balls—Li-atoms. Light blue—octahedra of M-cations and violet color—PO_4 tetraherda.

In these compounds, two phase transitions occur at different temperatures, with the high-temperature orthorhombic phase being the superionic one [55]. For $Li_3Sc_2(PO_4)_3$, the phase transition temperatures are 473 K and 573 K, whereas for $Li_3Fe_2(PO_4)_3$, these temperatures are 513 K and 573 K [56,57]. The lower temperature modifications (α and β) are characterized by the monoclinic space groups $P2_1/n$, whereas the structures of high-temperature γ-polymorphs in both cases are described in the frames of orthorhombic sp.gr. *Pcan*. Thus, the symmetry and the unit cell metrics of these compounds differ from the rhombohedral crystals of NASICON. However, the general configurations of mixed frameworks in both cases have many common features (Figure 17).

The main difference between α- and β-polymorphs lies in the arrangement of lithium atoms since the structure framework built by Sc(Fe)-octahedra and P-tetrahedra is only slightly more symmetrized in the β-phase than the framework of the α-phase. At room temperature, lithium atoms fully occupy (100%) three non-equivalent crystallographic positions, referred to as I, II, and III, in the voids of this structure type. Upon heating, the

third Li-position becomes less favorable than an additional one called the supplementary (Is) position.

In high-temperature γ-polymorph, lithium atoms experience further redistribution in comparison with the α- and β-phases. As a result of the phase transition, twelve lithium atoms of the unit cell are redistributed over three eight-fold crystallographic positions, whereas only one of them is fully occupied. Two other positions are occupied with lithium atoms only partially—for 25%. During phase transitions, the relative coordinates of M and P atoms remain almost unchanged. Thus, a significant difference between the arrangement of Li in the low-temperature and high-temperature forms of $Li_3Sc_2(PO_4)_3$ was revealed [54,55] (Figure 18). The reason for the anisotropy of the conductivity of lithium ions in these compounds becomes clear: in the superionic orthorhombic phase, the movement of Li along the *a*-axis will meet an obstacle in the form of a fully occupied site, whereas along the *c*-axis, its movement will be easier (Figure 18b).

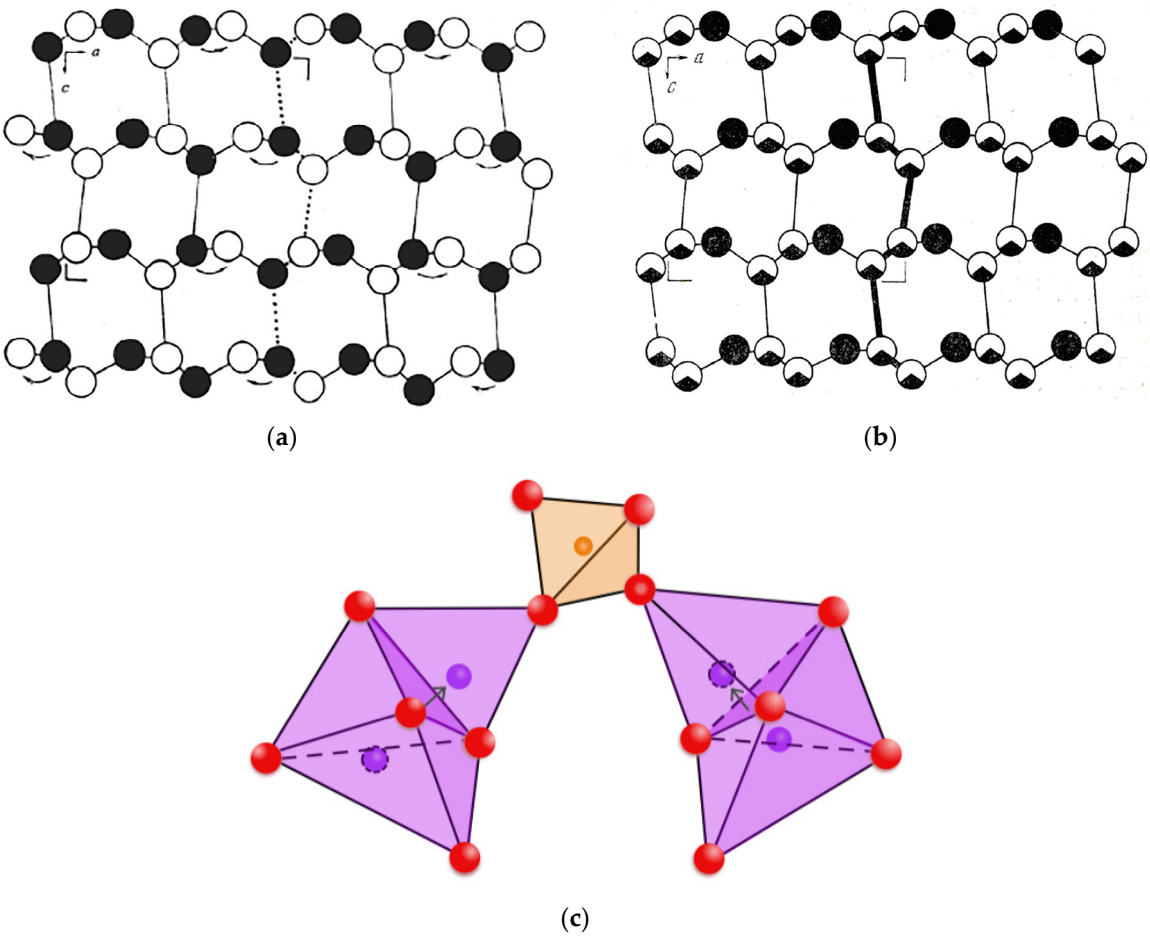

Figure 18. Scheme of lithium atoms arrangement in $Li_3Sc_2(PO_4)_3$ structures: (**a**) at 293 K, sp. gr. $P2_1/n$; (**b**) at 573 K, sp. gr. *Pcan*. The degree of filling of the circles corresponds to the degree of position occupancy (1 and 0.25). White circles are positions crystallographically possible but vacant. "Jump" of a Li atom from a trigonal bipyramid with 5-fold coordination to a tetrahedron with 4-fold coordination (**c**), adapted from [55]. The Li polyhedra and the PO_4 tetrahedron are highlighted in purple and brown, respectively. Red spheres are O atoms.

The lithium ionic conductivity in $Li_3Sc_2(PO_4)_3$ crystals at room temperature was found to be $1{\cdot}10^{-5}$ S·cm^{-1}, and in the superionic state, it increased ~10^3–10^4 times to $2{\cdot}10^{-2}$ S·cm^{-1} at T > 518 K [56].

Even at the early stages of the study of crystals with ionic conductivity, the question arose as to how cations, shifted from one polyhedron to the neighboring one, move within

a dense packing of anions, often directly touching each other. The problem, related to the displacement of Li atoms inside the structure, formulated at the beginning of this section, is explained in Figure 18c, which shows the passage of a Li^+ cation through a triangular face formed by three O^{2-} anions with short O-O ~2.5 Å distances.

Lithium-substituted lanthanum titanate $Li_{0,255}La_{0,582}TiO_3$ with the structural type of perovskite can serve as another illustration of the mysterious phenomenon associated with ion mobility [13]. At first glance, the crystal structure of $Li_{0.255}La_{0.582}TiO_3$ should not allow high ionic conductivity since the size of the conduction window is insufficient for unimpeded movement of Li^+ ions through channels inside the framework of TiO_3 octahedra (Figure 19). The observed contradiction can be explained by the special role of thermal vibrations of the framework atoms, due to which the size of the "conduction window" is constantly changing—the channels "breathe". The jump of ions to the neighboring position can occur at the moment of the greatest openness of the "window" [58].

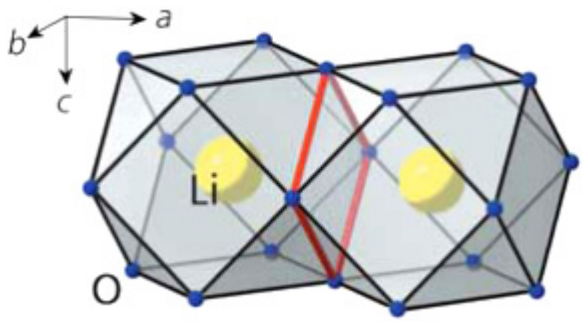

Figure 19. "Conductivity window" in $Li_{0.255}La_{0.582}TiO_3$—the narrowest section of the channel (rhombus highlighted in red bold line) for lithium-ion hopping from one position to the neighboring one, adapted from [13]. Blue balls are shown as O.

7. Conclusions

The ever-increasing consumption of electricity, coupled with decreasing fossil fuel resources, implies the search for alternative sources of electrical energy. In this process, the most important point is associated with the improvement of prospecting and technology of solid electrolytes [59]. The materials used in them are characterized by high ionic conductivity and, as shown above, are structural analogs of various minerals. The main conditions for fast ionic transport are related to the disorder in the positions occupied by the mobile ion and the presence of conduction channels running inside the structure. In accordance with these requirements, the search for new solid electrolytes is conducted along these two trends [1]. Their main property is the presence of positions available for the conducting ion, between which it could freely jump. For this purpose, it is necessary that these sites were not too distant from each other and were separated by a sufficiently wide "conduction window". As a rule, in an ideal crystal, all such positions are either fully occupied or completely free, which leads to the impossibility of ionic transport. That is why various heterovalent isomorphic impurities are introduced into the structure of a solid electrolyte to create partially occupied positions. The crystals obtained in this way are solid solutions from the point of view of solid-state chemistry and appear to be promising functional materials with ion-conducting properties. The results of their studies are dispersed in different editions, and the overview of new ideas related to their crystal structures was the focus of this paper.

Author Contributions: Conceptualization, D.P.; validation, D.P. and A.I.-S.; writing, original draft preparation, D.P.; writing, review, and editing, D.P. and A.I.-S. Both authors contributed equally. All authors have read and agreed to the published version of the manuscript.

Funding: This research received no external funding.

Acknowledgments: Authors thank all referees for their valuable comments, Mineral's Editors for their support, E.V. Antipov, L. Bindi for helpful discussions, and N.V. Zubkova for the preparation of several figures. Special gratitude is expressed to the publishers and authors for their permission to reproduce some figures.

Conflicts of Interest: The authors declare no conflicts of interest.

References

1. Ivanov-Schitz, A.K.; Murin, I.V. *Solid State Ionics*; SPb University: Sankt-Peterburg, Russia, 2000; Volume 1, 616p.
2. Faraday, M. *Experimental Researches in Electricity*; Art. 1339; Taylor and Francis: London, UK, 1839.
3. Sadovnikov, S.I.; Kostenko, M.G.; Gusev, A.I.; Lukoyanov, A.V. Low-Temperature Predicted Structures of Ag_2S (Silver Sulfide). *Nanomaterials* **2023**, *13*, 2638. [CrossRef] [PubMed]
4. Valeeva, A.A.; Sadovnikov, S.I.; Gusev, A.I. Polymorphic Phase Transformations in Nanocrystalline Ag_2S Silver Sulfide in a Wide Temperature Interval and Influence of Nanostructured Ag_2S on the Interface Formation in Ag_2S/ZnS Heteronanostructure. *Nanomaterials* **2022**, *12*, 1668. [CrossRef] [PubMed]
5. Blanton, T.; Misture, S.; Dontula, N.; Zdzieszynski, S. In Situ high-temperature X-ray diffraction characterization of silver sulfide, Ag_2S. *Powder Diffr.* **2011**, *26*, 114–118. [CrossRef]
6. Nernst, W. *Mutter Erde*; Spemann: Berlin, Germany, 1899; Volume 2, pp. 192–367.
7. Padma Kumar, P.; Yashonath, S. Ionic conduction in the solid state. *J. Chem. Sci.* **2006**, *118*, 135–154. [CrossRef]
8. Bu, X.; Feng, P. Superionic conductivity. In *Access Science*; McGraw Hill: New York, NY, USA, 2020. [CrossRef]
9. Knauth, P.; Tuller, H.L. Solid-State Ionics: Roots, Status, and Future Prospects. *J. Am. Ceram. Soc.* **2002**, *85*, 1654–1680. [CrossRef]
10. Khasanova, N.; Drozhzhin, O.; Yakubovich, O.; Antipov, E. Mineral inspired electrode materials for metal-ion batteries. In *Reference Module in Chemistry, Molecular Sciences and Chemical Engineering*, 3rd ed.; Elsevier Ltd.: Amsterdam, The Netherlands, 2023; Chapter 7.2; pp. 363–403.
11. Yakubovich, O.; Khasanova, N.; Antipov, E. Mineral-Inspired Materials: Synthetic Phosphate Analogues for Battery Applications. *Minerals* **2020**, *10*, 524. [CrossRef]
12. Pushcharovsky, D.Y. *Structures and Properties of Crystals*; GEOS: Moscow, Russia, 2022; 260p.
13. Ivanov-Schitz, A.K.; Dem'yanets, L.N. Materials for solid state ionics. *Priroda* **2003**, *12*, 35–43.
14. Fedotov, S.S.; Samarin, A.S.; Antipov, E.V. $KTiOPO_4$-structured electrode materials for metal-ion batteries: A review. *J. Power Sources* **2020**, *480*, 228840. [CrossRef]
15. Maczka, M.; Sieradzki, A.; Poprawski, R.; Hermanowicz, K.; Hanuza, J. Lattice dynamics calculations and temperature dependence of vibrational modes of ferroelastic Li_2TiGeO_5. *J. Phys. Condens. Matter.* **2006**, *18*, 2137–2147. [CrossRef]
16. Kireev, V.V.; Yakubovich, O.V.; Ivanov-Shits, A.K.; Mel'nikov, O.K.; Dem'yanets, L.N.; Chaban, N.G. Growth, Structure, and Electrophysical Properties of Single Crystals of A_2TiGeO_5 (A = Li and Na). *Russ. J. Coord. Chem.* **2001**, *27*, 31–37. [CrossRef]
17. Bindi, L.; Evain, M.; Pradel, A.; Albert, S.; Ribes, M.; Menchetti, S. Fast ion conduction character and ionic phase-transitions in disordered crystals: The complex case of the minerals of the pearceite–polybasite group. *Phys. Chem. Miner.* **2006**, *33*, 677–690. [CrossRef]
18. Bindi, L.; Evain, M.; Menchetti, S. Complex Twinning, Polytypism and Disorder Phenomena in the Cristal Structures of Antimonpearceite and Arsenpolybasite. *Canad. Miner.* **2007**, *45*, 321–333. [CrossRef]
19. Withers, R.L.; Norén, L.; Welberry, T.R.; Bindi, L.; Evain, M.; Menchetti, S. A composite modulated structure mechanism for Ag^+ fast ion conduction in pearceite and polybasite mineral solid electrolytes. *Solid State Ion.* **2008**, *179*, 2080–2089. [CrossRef]
20. Maksimov, B.A.; Kharitonov, Y.A.; Belov, N.V. Crystal structure of the Na,Y-metasilicate $Na_5YSi_4O_{12}$. *Sov. Phys. Dokl.* **1974**, *18*, 763–765.
21. Maksimov, B.A.; Belov, N.V. High-temperature X-ray studies of $Na_5YSi_4O_{12}$ single crystals. *Sov. Phys. Dokl.* **1981**, *26*, 1026–1029.
22. Shannon, R.D.; Taylor, B.E.; Gier, T.E.; Chen, H.Y.; Berzins, T. Ionic conductivity in sodium yttrium silicon oxide ($Na_5YSi_4O_{12}$)-type silicates. *Inorg. Chem.* **1978**, *17*, 958–964. [CrossRef]
23. Pushcharovsky, D.Y.; Karpov, O.G.; Pobedimskaya, E.A.; Belov, N.V. The crystal structure of $K_3NdSi_6O_{15}$. *Sov. Phys. Dokl.* **1977**, *22*, 292–293.
24. Jeffery, A.J.; Gertisser, R.; Jackson, R.A.; O'Driscoll, B.; Kronz, A. On the compositional variability of dalyite, $K_2ZrSi_6O_{15}$: A new occurrence from Terceira, Azores. *Mineral. Mag.* **2016**, *80*, 547–565. [CrossRef]
25. Haile, S.M.; Wuench, B.J.; Laudise, R.A.; Opila, R.; Siegrist, T.; Foxman, B.M. Crystallography and Composition of Some New Potassium-Neodimium Silicates. *Trans. ACA* **1991**, *27*, 77–94.
26. Haile, S.M.; Wuensch, B.J.; Siegrist, T.; Laudise, R.A. Conductivity and crystallography of new alkali rare-earth silicates synthesized as possible fast-ion conductors. *Solid State Ion.* **1992**, *53–56*, 1292–1301. [CrossRef]
27. Popović, L.; Manoun, B.; de Waal, D.; Nieuwoudt, M.K.; Comins, J.D. Raman spectroscopic study of phase transitions in Li_3PO_4. *J. Raman Spectrosc.* **2003**, *34*, 77–83. [CrossRef]
28. Ayu, N.I.P.; Kartini, E.; Prayogi, L.D.; Faisal, M.; Supardi, Z. Crystal structure analysis of Li_3PO_4 powder prepared by wet chemical reaction and solid-state reaction by using X-ray diffraction (XRD). *Ionics* **2016**, *22*, 1051–1057. [CrossRef]

29. Zhang, L.; Malys, M.; Jamroz, J.; Krok, F.; Wrobel, W.; Hull, S.; Yan, H.; Abrahams, I. Structure and Conductivity in LISICON Analogues within the Li_4GeO_4–Li_2MoO_4 System. *Inorg. Chem.* **2023**, *62*, 11876–11886. [CrossRef]
30. Szlugaj, J.; Radwanek-Bąk, B. Lithium sources and their current use. *Gospod. Surowcami Miner.—Miner. Resour. Manag.* **2022**, *38*, 61–88.
31. Zhao, G.; Suzuki, K.; Okumura, T.; Takeuchi, T.; Masaaki, H.; Kanno, R. Extending the Frontiers of Lithium-Ion Conducting Oxides: Development of Multicomponent Materials with γ-Li_3PO_4-Type Structures. *Chem. Mater.* **2022**, *34*, 3948–3959. [CrossRef]
32. Ksenofontov, D.A.; Zubkova, N.V.; Pushcharovsky, D.Y.; Dem'yanets, L.N.; Kolitsch, U.; Tillmanns, E.; Ivanov-Shitz, A.K. Synthesis and crystal structure of $Li_{3.17}(P_{0.69}Ge_{0.24}Mo_{0.07})O_4$. *Crystallogr. Rep.* **2006**, *51*, 391–394. [CrossRef]
33. Drozhzhin, O.A.; Sobolev, A.V.; Sumanov, V.D.; Glazkova, I.S.; Aksyonov, D.A.; Grebenshchikova, A.D.; Tyablikov, O.A.; Alekseeva, A.M.; Mikheev, I.V.; Dovgaliuk, I.; et al. Exploring the Origin of the Superior Electrochemical Performance of Hydrothermally Prepared Li-Rich Lithium Iron Phosphate $Li_{1+\delta}Fe_{1-\delta}PO_4$. *J. Phys. Chem. C* **2020**, *124*, 126–134. [CrossRef]
34. Wang, B.; Chen, S.C.; Greenblatt, M. The Crystal Structure and Ionic Conductivity of the Ilmenite Polymorph of $NaSbO_3$. *J. Solid State Chem.* **1994**, *108*, 184–188. [CrossRef]
35. Olmi, F.; Sabelli, C. Brizziite, $NaSbO_3$, a new mineral from the Cetine mine (Tuscany, Italy): Description and crystal structure. *Eur. J. Miner.* **1994**, *6*, 667–672. [CrossRef]
36. Spiegelberg, P. X-ray studies on potassium antimonates. *Ark. Kemi. Mineral. Geol.* **1940**, *A14*, 1–12.
37. Hong, H.Y.-P.; Kafalas, J.A.; Goodenough, J.B. Crystal chemistry in the system $MSbO_3$. *J.Solid State Chem.* **1974**, *9*, 345–351. [CrossRef]
38. Ramírez-Meneses, E.; Chavira, E.; Domínguez-Crespo, M.A.; Escamilla, R. Synthesis and characterization of $NaSbO_3$ compound. *Superf. Y Vacío* **2007**, *20*, 14–18.
39. Mizoguchi, H.; Woodward, P.M.; Byeon, S.-H.; Parise, J.B. Polymorphism in $NaSbO_3$: Structure and Bonding in Metal Oxides. *J. Am. Chem. Soc.* **2004**, *126*, 3175–3184. [CrossRef] [PubMed]
40. Hong, H.Y.-P. New solid electrolytes. In *Solid State Chemistry of Energy Conversion and Storage*; Goodenough, J.B., Whittingham, M.S., Eds.; American Chemical Society: Washington, DC, USA, 1977; p. 179.
41. Chi, C.; Katsui, H.; Goto, T. Effect of Li addition on the formation of Na-β/β''-alumina film by laser chemical vapor deposition. *Ceram. Int.* **2017**, *43*, 1278–1283. [CrossRef]
42. Kim, D.-G.; Moosavi-Khoonsari, E.; Jung, I.-H. Thermodynamic modeling of the K_2O-Al_2O_3 and K_2O-MgO-Al_2O_3 systems with emphasis on β- and β''-aluminas. *J. Eur. Ceram. Soc.* **2018**, *38*, 3188–3200. [CrossRef]
43. Collin, G.; Boilot, J.P.; Colomban, P.; Comes, R. Host lattices and superionic properties in β- and β''-alumina. I. Structures and local correlations. *Phys. Rev. B* **1986**, *34*, 5838–5849. [CrossRef] [PubMed]
44. McWhan, D.B.; Dernier, P.D.; Vettier, C.; Cooper, A.S.; Remeika, J.P. X-ray diffuse scattering from alkali, silver, and europium β-alumina. *Phys. Rev. B* **1978**, *17*, 4043–4059. [CrossRef]
45. Krüger, B.; Galuskin, E.V.; Galuskina, I.O.; Hannes Krüger, H.; Vapnik, Y. Kahlenbergite $KAl_{11}O_{17}$, a new β-alumina mineral and Fe-rich hibonite from the Hatrurim Basin, the Negev desert, Israel. *Eur. J. Mineral.* **2021**, *33*, 341–355. [CrossRef]
46. Hong, H. Y-P. Crystal structures and crystal chemistry in the system $Na_{1+x}Zr_2Si_xP_{3-x}O_{12}$. *Mater. Res. Bull.* **1976**, *11*, 173–182. [CrossRef]
47. Goodenough, J.B.; Hong, H.Y.-P.; Kafalas, J.A. Fast Na^+-ion Transport in Skeleton Structures. *Mater. Res. Bull.* **1976**, *11*, 203–220. [CrossRef]
48. Wang, J.; He, T.; Yang, X.; Cai, Z.; Wang, Y.; Lacivita, V.; Kim, H.; Ouyang, B.; Ceder, G. Design principles for NASICON super-ionic conductors. *Nat. Commun.* **2023**, *14*, 5210. [CrossRef] [PubMed]
49. Park, S.; Chotard, J.-N.; Carlier, D.; Moog, I.; Courty, M.; Duttine, M.; Fauth, F.; Iadecola, A.; Croguennec, L.; Masquelier, C. Crystal Structures and Local Environments of NASICON-Type $Na_3FeV(PO_4)_3$ and $Na_4FeV(PO_4)_3$ Positive Electrode Materials for Na-Ion Batteries. *Chem. Mater.* **2021**, *33*, 5355–5367. [CrossRef]
50. Deng, Z.; Mishra, T.P.; Mahayoni, E.; Ma, Q.; Tieu, A.J.K.; Guillon, O.; Chotard, J.-N.; Seznec, V.; Cheetham, A.K.; Masquelier, C.; et al. Fundamental investigations on the sodium-ion transport properties of mixed polyanion solid-state battery electrolytes. *Nat. Commun.* **2022**, *13*, 4470. [CrossRef] [PubMed]
51. Pinus, I.Y. Investigation of Cation Mobility in Materials with NACICON Structure, $A_{1-X}Zr_{2-X}Nb_X(PO_4)_3$ (A = Li, H). Ph.D. Thesis, Higher Chemical College of RAS, N.S. Kurnakov Institute of General and Inorganic Chemistry of RAS, Moscow, Russia, 2009.
52. Bnownfield, M.-E.; Foord, E.E.; Sutley, S.J.; Botinelly, T. Kosnarite, $KZr_2(PO_4)_3$, a new mineral from Mount Mica and Black Mountain, Oxford County, Maine. *Amer. Mineral.* **1993**, *78*, 653–656.
53. Asabina, E.A.; Pet'kov, V.I.; Rusakov, D.A.; Lazoryak, B.I.; Kurazhkovskaya, V.S. The study of the crystalline phosphates of kosnarite type structure containing different alkali metals. *J. Solid State Chem.* **2010**, *183*, 1980–1984. [CrossRef]
54. Genkina, E.A.; Muradyan, L.A.; Maksimov, B.A. Crystal Structure of the Monoclinic Modification of $Li_3Sc_2(PO_4)_3$ at 293 K. *Sov. Phys. Crystallogr.* **1986**, *31*, 350–351.
55. Maksimov, B.A.; Muradyan, L.A.; Genkina, E.A.; Verin, I.A. Crystal Structure of $Li_3Sc_2(PO_4)_3$ at 573 K. *Sov. Phys. Crystallogr.* **1986**, *31*, 348–349.
56. Bykov, A.B.; Chirkin, A.P.; Demyanets, L.N.; Doronin, S.N.; Genkina, E.A.; Ivanov-Schitz, A.K.; Kondratyuk, I.P.; Maksimov, B.A.; Mel'nikov, O.K.; Muradyan, L.N.; et al. Superionic Conductors $Li_3M_2(PO_4)_3$ (M = Fe. Sc, Cr): Synthesis, Structure and Electrophysical Propeties. *Solid State Ion.* **1990**, *38*, 31–52. [CrossRef]

57. Ivanov-Schitz, A.K.; Schoonman, J. Electrical and interfacial properties of a $Li_3Fe_2(PO_4)_3$ single crystal with silver electrodes. *Solid State Ion.* **1996**, *91*, 93–99. [CrossRef]
58. Inaguma, Y.; Katsumata, T.; Itoh, M.; Morii, Y.; Tsurui, T. Structural investigations of migration pathways in lithium ion-conducting $La_{2/3-x}Li_{3x}TiO_3$ perovskites. *Solid State Ion.* **2006**, *177*, 3037–3044. [CrossRef]
59. Larcher, D.; Tarascon, J.-M. Towards greener and more sustainable batteries for electrical energy storage. *Nat. Chem.* **2014**, *7*, 19–29. [CrossRef] [PubMed]

Disclaimer/Publisher's Note: The statements, opinions and data contained in all publications are solely those of the individual author(s) and contributor(s) and not of MDPI and/or the editor(s). MDPI and/or the editor(s) disclaim responsibility for any injury to people or property resulting from any ideas, methods, instructions or products referred to in the content.